HHS Public Access

Author manuscript

Cell Rep. Author manuscript; available in PMC 2017 December 13.

Published in final edited form as:

Cell Rep. 2017 November 21; 21(8): 2104–2117. doi:10.1016/j.celrep.2017.10.094.

Caveolin-1 is required for Th1 cell infiltration but not tight junction remodeling at the blood-brain barrier in autoimmune neuroinflammation

Sarah E. Lutz[1,7,8], **Julian R. Smith**[1], **Dae Hwan Kim**[5], **Carl V. L. Olson**[5], **Kyle Ellefsen**[5], **Jennifer M. Bates**[6], **Sunil P. Gandhi**[5], and **Dritan Agalliu**[1,2,3,4,8]

[1]Department of Neurology, Columbia University Medical Center, New York, NY 10032, USA

[2]Department of Pathology & Cell Biology, Columbia University Medical Center, New York, NY 10032, USA

[3]Department of Pharmacology, Columbia University Medical Center, New York, NY 10032, USA

[4]Columbia Translational Neuroscience Initiative, Columbia University Medical Center, New York, NY 10032, USA

[5]Department of Neurobiology and Behavior, University of California, Irvine, CA 92697, USA

[6]Institute for Immunology, University of California, Irvine, CA 92697, USA

SUMMARY

Lymphocytes cross vascular boundaries via either disrupted tight junctions (TJs) or caveolae to induce tissue inflammation. In the central nervous system (CNS), Th17 lymphocytes cross the blood-brain barrier (BBB) prior to Th1 cells, yet this differential crossing is poorly understood. We have used intravital two-photon imaging of the spinal cord in wild-type and caveolae-deficient mice with fluorescently labeled endothelial TJs, to determine how TJ remodeling and caveolae regulate CNS entry of lymphocytes during the experimental autoimmune encephalomyelitis (EAE) model for multiple sclerosis. We find that dynamic TJ remodeling occurs early in EAE but does not depend upon caveolar transport. Moreover, Th1 but not Th17 lymphocytes are significantly reduced in the inflamed CNS of mice lacking caveolae. Therefore, TJ remodeling facilitates Th17 migration across the BBB, whereas caveolae promote Th1 entry into the CNS. Moroever, therapies

[8]Correspondence: Dritan Agalliu Ph.D. (da191@cumc.columbia.edu) or Sarah E. Lutz Ph.D. (selutz@uic.edu).
[7]Current address: Department of Anatomy and Cell Biology, University of Illinois at Chicago College of Medicine, Chicago, IL 60612, USA.
Lead Contact: Dritan Agalliu Ph.D. da191@cumc.columbia.edu; phone: 212-305-0323.
Address: Department of Neurology, Columbia University Medical Center, 650 W. 168th Street, William Black Building Room 310E, New York, NY 10032; Phone: 212-305-0323; Fax: 212-305-0241.

AUTHOR CONTRIBUTIONS

Conceptualization, S.E.L., S.P.G., D.A.; Investigation, S.E.L., J.R.S., D.H.K., C.V.L.O., K.E., J.M.B. D.A.; Resources, S.P.G., D.A.; Writing – Original Draft, S.E.L., S.P.G., D.A; Writing – Review and Editing, S.E.L., D.A.; Supervision, S.E.L., S.P.G., D.A.; Funding, S.E.L., S.P.G., D.A..

that target both TJ degradation and caveolar transcytosis may limit lymphocyte infiltration during inflammation.

eTOC BLURB

Autoreactive T cell trafficking into the CNS exacerbates multiple sclerosis, yet how these cells enter the CNS remains unclear. Lutz *et al.* demonstrate that Caveolin1 exacerbates disease pathogenesis by promoting selective trafficking of Th1 cells across the BBB independently of tight junction remodeling.

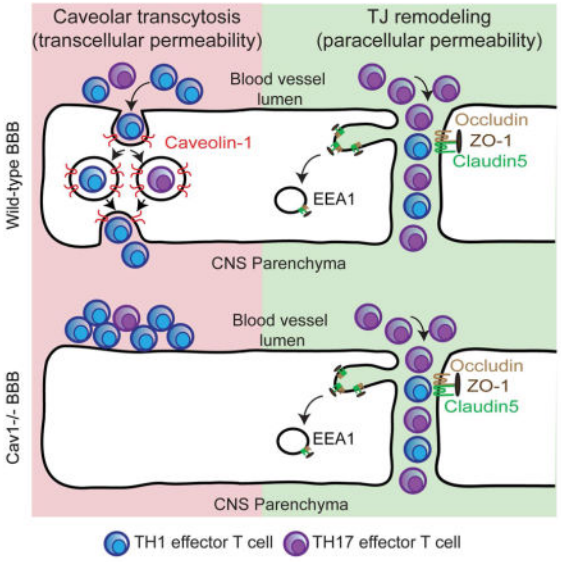

Keywords

multiple sclerosis; experimental autoimmune encephalomyelitis; blood-brain barrier; endothelium; tight junction; caveolae; transcytosis; Claudin5; Caveolin1; intravital microscopy

INTRODUCTION

During inflammation, immune cells cross blood vessels of multiple organs to mount an appropriate immune response. Immune cell trafficking across blood vessels is controlled by both cell junctions and vesicles that regulate transport between or within endothelial cells (Komarova et al., 2017). During CNS autoimmune diseases, leukocytes migrate across several pathways to reach the CNS parenchyma. These include a vascular route through the blood-brain barrier (BBB)/blood-spinal cord barrier (BSCB), the blood-cerebrospinal fluid route through an epithelial barrier present in the choroid plexus and the meningeal lymphatic route on the surface of the brain (Daneman and Engelhardt, 2017; Louveau et al., 2017; Platt et al., 2017). The BBB is characterized by impermeable tight junctions (TJ) and reduced transcellular transcytosis (Lampugnani et al., 2015; Reese and Karnovsky, 1967). Immune cells can extravasate through either TJs (paracellular migration) or endothelial vesicles (transcellular migration) (Engelhardt and Wolburg, 2004; Martinelli et al., 2014). Among the various immune cell subtypes, Th1 and Th17 lymphocytes are distinguished by unique

effector cytokines that damage axons, oligodendrocytes, and the neurovasculature (Rostami and Ciric, 2013; Simmons et al., 2014; Stromnes et al., 2008). Moroever, Th17 cells enter into the CNS prior to Th1 cells in EAE (Murphy et al., 2010; Rothhammer et al., 2011). However it is unknown whether they employ similar or distinct mechanisms to cross endothelial barriers.

Claudin3, 5, 12 and Occludin are critical junctional proteins that normally restrict paracellular movement of small molecules across endothelial cell barriers (Nag, 2003; Nitta et al., 2003). These proteins are disrupted in inflammatory diseases including multiple sclerosis (MS) and its animal model experimental autoimmune encephalomyelitis (EAE) (Bennett et al., 2010; Kirk et al., 2003). TJ disruption precedes overt lesion formation and correlates with clinical severity of EAE (Alvarez et al., 2015; Fabis et al., 2008). Moreover, endothelial TJ degradation promotes paracellular leukocyte migration (Reijerkerk et al., 2008; Winger et al., 2014), whereas overexpression of Claudin1 is protective for EAE (Pfeiffer et al., 2011). Endothelial TJs also prevent serum proteins such as fibrinogen from crossing the BBB, thereby conferring disease protection (Ryu et al., 2015). TJs are highly dynamic *in vivo*, in both the cerebral cortex and intestinal epithelia, and their turnover is increased during inflammation (Knowland et al., 2014; Marchiando et al., 2010). Although barrier disruption promotes neuroinflammation by enabling inflammatory proteins and leukocytes to access the CNS, how dynamic remodeling of TJs correlates with disease pathogenesis and its importance for immune cell trafficking remains unclear.

A second mechanism controlling BBB permeability is endocytic/transcytotic transport. In the CNS endothelium, most endocytic vesicles are non-clathrin-coated caveolae containing Caveolin1 (Cav1) (Kovtun et al., 2015; Nag, 2003). Both expression of Cav1 (Shin et al., 2005; Wu et al., 2016) and the density of endocytotic vesicles in CNS endothelium increase during acute MS and EAE (Brown, 1978; Claudio and Brosnan, 1992). Endothelial caveolae may provide a migratory route for myelin-specific T cells into the CNS (Raine et al., 1990), due to clustering of adhesion molecules (Carman and Martinelli, 2015; Millan et al., 2006). Caveolar activity also enhances leukocyte migration across the meninges (Santizo et al., 2002). Caveolae regulate cytokine-induced TJ turnover in epithelial and endothelial cells (Marchiando et al., 2010; Stamatovic et al., 2009; Sun et al., 2009). However, how caveolae regulate Th17 versus Th1 T cell trafficking and TJ remodeling at the BBB during EAE is poorly understood.

Here we examine how BBB components are disrupted *in vivo* during EAE, and which routes are used by distinct effector T cell subtypes to enter the CNS. We use intravital two-photon microscopy in *Tg eGFP-Claudin5*$^{+/-}$ mice (Knowland et al., 2014) to visualize dynamic changes in TJs at the BSCB during EAE. We find that TJ remodeling precedes onset of disease and barrier permeability. Moreover, mice that lack caveolae have reduced EAE clinical severity and a selective decrease in BSCB permeability to Th1 cells, yet display no changes in dynamic TJ remodeling. These findings suggest that during neuroinflammation, caveolae-independent TJ remodeling facilitates Th17 lymphocyte transmigration across the BBB, whereas caveolae regulate the entry of Th1 lymphocytes into the CNS.

RESULTS

Live imaging of TJ structural changes in healthy spinal cord vessels

To document real-time changes in TJ structure in the spinal cord microvasculature during EAE, we used intravital two-photon microscopy in *Tg eGFP-Claudin5*$^{+/-}$ transgenic mice that express a fusion of enhanced green fluorescent protein (eGFP) to Claudin5 in endothelial cells (Knowland et al., 2014). We performed dorsal laminectomy at lumbar level 1 (L1) to expose the spinal cord and time-lapse imaging of endothelial TJs over 45-minute intervals (Fig. 1A,B; n = 6–7 mice/group). We focused on post-capillary venules because leukocyte transmigration occurs primarily in such vessels during EAE and is associated with loss of Claudin5 (Paul et al., 2013). In healthy mice, eGFP-positive TJs are mostly linear (Fig. 1E,F). 25% of TJs in healthy blood vessels in the dorsal white matter show protrusions (bulbous extensions of 1–5 μm extending from the major TJ segment axis), however only 5% of protrusions rapidly remodel (appear or disappear during imaging) (Fig. 1C,E,F,M,N and Movie S1). Moreover, healthy TJs exhibit few gaps (1.8%, Fig. 1D–F,O) or tortuous, irregular non-linearity (4.6%; Fig. 1C,P), which are reminiscent of junctions in cells lacking ZO-1 and -3 proteins (Umeda et al., 2006). Only 5% of endothelial TJ segments undergo dynamic remodeling in the healthy spinal cord.

Dynamic remodeling of TJs precede disease onset and barrier permeability during EAE

We next asked how TJ remodeling correlates with BBB permeability during EAE. We induced active $MOG_{35–55}$ EAE (Lutz et al., 2012) in *Tg eGFP-Claudin5*$^{+/-}$ mice, and assessed TJ structure by two-photon microscopy at three stages of disease: 1) prior to clinical signs (EAE score 0, 6–7 days post-immunization [dpi]), 2) in mice with tail paralysis (score 1, 10 dpi), and 3) in mice with hind limb weakness/paralysis (score 2–3, 13–15 dpi). All animals with EAE have significantly more protrusions than healthy controls (i.e. ~70% all stages of EAE versus ~25% in controls (Fig. 1G–M; $p<0.001$, one-way ANOVA with Tukey's multiple comparison). Approximately 40% of TJ protrusions in post-capillary venules during EAE undergo rapid remodeling (Fig. 1G–N and Movie S2). Similarly, TJ segments with gaps and tortuous segments are predominant at EAE scores 1 (55.8% and 56.2%, respectively) and 2 (56.5% and 64.6%, respectively), but these defects are absent in mice prior to onset of clinical signs (14.5% and 14.3% score 0; Fig. 1G–L,O,P and data not shown). Therefore, TJ dynamic remodeling precedes gap formation. Internalized TJ protrusions localize *in vivo* with the early endosome marker EEA-1, but not clathrin (Fig. S1). Similar to healthy mice, CFA/pertussis toxin-treated control mice, which do not develop disease, exhibit only static (50%) but not dynamic (7.7%) protrusions in TJ segments, with few gaps (3.7%) or irregular segments (10%); these frequencies are similar to those in healthy mice (Fig. 1M–P). Thus, TJ dynamic remodeling and instability are a feature of active EAE.

Caveolin-1 is not required for TJ structural changes in EAE spinal cord vessels

TJ stability may be regulated by caveolae, a class of membrane invaginations that require Cav1 (Cheng and Nichols, 2016). Caveolae regulate endocytosis of TJ proteins and barrier permeability in brain endothelial cells *in vitro* (Song et al., 2007; Stamatovic et al., 2009), however it is unknown if caveolae perform similar functions at the BBB *in vivo*. To address

this, we immunized *Cav1*$^{-/-}$ mice (Razani et al., 2001) with $MOG_{35–55}$ and assessed disease and TJ remodeling. EAE-induced *Cav1*$^{-/-}$ mice showed reduced disease severity compared to wild-type (WT) littermates (n = 34 wild-type, n = 32 *Cav1*$^{-/-}$; $p<0.01$, two-way repeated measure ANOVA with Sidak's multiple comparison test; Fig. 2A). The maximum score attained by *Cav1*$^{-/-}$ mice was lower than WT mice ($p<0.001$, Mann-Whitney comparison of medians) despite similar disease incidence (Fig. 2B,C). The peripheral immune response to MOG was unchanged in *Cav1*$^{-/-}$ mice compared to WT mice (Fig. S2A–K), consistent with a recent report (Wu et al., 2016). In a subset of animals examined up to 25 days post-immunization, the clinical trend remained the same (Fig. S2L, n = 5 per group, $p<0.001$). *Cav1*$^{-/-}$ mice with EAE had slightly better myelin preservation in the thoracic spinal cord than wild-type mice with EAE (Fig. S2M–O). However, there was no difference in oligodendrocyte apoptosis (Fig. S2P–R) suggesting that caveolae do not influence oligodendrocyte death.

Caveolae are not required *in vivo* during EAE for TJ dynamic remodeling and permeability to small molecules

We used intravital two-photon microscopy to compare TJ dynamic remodeling *in vivo* between *Tg eGFP-Claudin5*$^{+/-}$ *Cav1*$^{-/-}$ and *Tg eGFP-Claudin5*$^{+/-}$ mice at an early stage of EAE (score 0, 7 dpi), when we first observe TJ dynamic remodeling (Fig. 1G,H,M–P). *Tg eGFP-Claudin5*$^{+/-}$ *Cav1*$^{-/-}$ and *Tg eGFP-Claudin5*$^{+/-}$ mice had similar frequencies of static and dynamic protrusions, gaps or tortuosities (Fig. 2D–I). To correlate TJ structural changes with loss of BSCB function *in vivo*, we injected *Tg eGFP-Claudin5*$^{+/-}$ EAE, *Tg eGFP-Claudin5*$^{+/-}$ *Cav1*$^{-/-}$ EAE, CFA/pertussis toxin controls, and healthy mice intravenously with 5-(and-6-) tetramethylrhodamine biocytin (biocytin-TMR, 869 Da), which crosses the BBB when TJs are disrupted (Dileepan et al., 2016; Knowland et al., 2014; Lengfeld et al., 2017). We visualized biocytin-TMR in the spinal cord by two-photon microscopy, then normalized it *ex vivo* to liver accumulation from the same animal (Fig. 3). The tracer is retained within blood vessels in healthy and CFA-treated mice (Fig. 3A–D,M,N). Leakage from vessels is mild at EAE score 0 (Fig. 3E–F,M,N) and pronounced in symptomatic mice, particularly at sites of TJ gaps (scores 1–3; Fig. 3G–J,M,N). However, there is no difference in biocytin leakage across the BSCB between *Tg eGFP-Claudin5*$^{+/-}$ *Cav1*$^{-/-}$ and *Tg eGFP-Claudin5*$^{+/-}$ mice (Fig. 3K–N).

We also measured parenchymal deposition of the serum protein fibrinogen (approximately 340 kDa) by immunofluorescence. Fibrin accumulation was minimal in CFA/Ptx controls and EAE score 0–1 mice (Fig. S3A–I,P,Q). Mice with clinical EAE scores >2 had significantly elevated fibrinogen at thoracic and lumbar levels of the spinal cord (Fig. S3J–L,P–Q), with regions of leukocyte infiltration displaying greatest leakage (Fig. S3I,L,O). *Tg eGFP-Claudin5*$^{+/-}$ *Cav1*$^{-/-}$ EAE mice and *Tg eGFP-Claudin5*$^{+/-}$ EAE mice have similar levels of fibrinogen leakage (Fig. S3M–Q), consistent with tracer leakage across the BSCB. Thus, the presence of TJ gaps correlates closely with paracellular BSCB permeability in both *Tg eGFP-Claudin5*$^{+/-}$ EAE mice and *Tg eGFP-Claudin5*$^{+/-}$ *Cav1*$^{-/-}$ EAE mice.

We next measured leakage of albumin-AlexaFluor 594, a 66 kDa protein that can undergo caveolar transcytosis (Tiruppathi et al., 1997), during active $MOG_{35–55}$ EAE in wild-type

and *Cav1*$^{-/-}$ mice. We used confocal microscopy to assess endothelial- and parenchymal-associated albumin (Knowland et al., 2014; Lengfeld et al., 2017). Healthy and CFA/Ptx control mice exhibit minimal albumin-AlexaFluor 594 uptake into both lumbar and thoracic spinal cords (Fig. 4A–D,M,N and Fig S4A,B) consistent with previous studies (Al-Izki et al., 2012; Tonra et al., 2001). Both endothelial- and parenchyma-associated albumin are significantly increased at EAE scores 2–3.5 (Fig. 4G,H,M,N). Albumin transport across the endothelium depends on caveolar transcytosis in some peripheral tissues and during ischemic stroke in the brain (Knowland et al., 2014; Razani et al., 2001). As expected, the absence of Cav1 prevents albumin leakage in spinal cords of healthy mutant mice (Fig. 4I,J,M,N and Fig. S4A,B). However, *Cav1*$^{-/-}$ mice with EAE have levels of endothelium- or parenchymal-associated albumin similar to their wild-type littermates using score-matched EAE mice (Fig. 3K–N). Thus, BSCB permeability to larger molecules such as albumin increases at severe EAE through caveolae-independent routes.

Loss of Caveolin-1 selectively reduces Th1 cell infiltration into the CNS

We tested the role of caveolar transcytosis in T cell diapedesis. In contrast with a recent study (Wu et al., 2016), we found that *Cav1*$^{-/-}$ mice with EAE have similar CD4^{+} T cell numbers in both meningeal and parenchymal compartments 15 dpi compared to wild-type mice with EAE by immunostaining (Fig. 5A–G; two-way Student's t-test). To understand how loss of Cav1 reduces the severity of EAE, we examined lymphocyte subtypes in the spinal cord using flow cytometry. We found that although the total number of infiltrating T and B cells were similar between wild-type and *Cav1*$^{-/-}$ mice with EAE, the ratio of Th1 to Th17 subtypes was significantly altered (Fig. 5H–Q). Spinal cords of *Cav1*$^{-/-}$ mice had a selective decrease in IFN-γ-producing Th1 cells and increased IL-17A-producing Th17 cells (Fig. 5I,J,N,O). No differences were found for IL-17A^{+} IFNγ^{+} doubly-positive cells (Fig. 5P) nor CD19^{+} B-cells (Fig. 5K,Q). To confirm these findings, we assessed transmigration of Th1- or Th17-enriched populations of T cells (Fig. S5A–C) across cultured primary brain endothelial cell (BECs) monolayers from either wild-type or *Cav1*$^{-/-}$ mice (Fig. 6). We found that the *Cav1*$^{-/-}$ endothelium showed a 93.5% reduction in transcellular transmigration and 49% reduction in paracellular transmigration of Th1 lymphocytes (*p<0.05; Fig. 6A–E, J). The caveolae inhibitor methyl-β cyclodextrin (MβCD) also suppressed Th1 transcellular transmigration across WT BECs (Fig. S5D–G). Consistent with our findings *in vivo*, there was no impairment in Th17 lymphocyte migration across *Cav1*$^{-/-}$ endothelium (Fig. 6F–J). Thus, caveolae play an important role in allowing Th1 cell entry into the CNS during neuroinflammation, whereas Th17 cells primarily enter the CNS via disrupted TJs. Furthermore, caveolae are not required for dynamic remodeling of TJs or vascular permeability in EAE.

DISCUSSION

In this study, we have examined *in vivo* dynamic remodeling of TJs at the BSCB in healthy living mice and during the EAE model of MS. We find that TJs in post-capillary venules of the spinal cord are mostly stable in healthy mice (Fig. 1M–P); however, dynamic remodeling of TJs and paracellular BSCB leakage increase prior to onset of EAE and remain high throughout disease. Moreover, endothelial TJs rapidly remodel independently of caveolae in

neuroinflammation, because TJs exhibit similarly dynamic behavior in both wild-type and *Cav1*$^{-/-}$ EAE mice. Finally, we demonstrate that caveolae are essential for transmigration of IFN-γ-producing Th1 cells into the spinal cord during EAE. We discuss the cell biological mechanisms underlying BBB dysfunction in neurological diseases, mechanisms of immune cell infiltration into the CNS through paracellular and transcellular pathways and the relevance for EAE progression.

Multiple studies have suggested that endothelial barriers of the brain, spinal cord, meninges, and choroid plexus are functionally distinct from each other and from those of peripheral vasculature. The BBB and BSCB differ both in expression of barrier-specific proteins and their functional permeability. Compared to brain, endothelial cells in the spinal cord have decreased adherens junction (AJ) (e.g. Cadherin-5, α–, β–, γ-catenin) and TJ (e.g. Occludin, ZO-1) proteins, and a corresponding increase in permeability to low-molecular-weight tracers (Bartanusz et al., 2011). Our intravital imaging studies reveal that TJs in white matter spinal cord are ~ four fold more dynamic (Fig. 1) than those in the cortex (Knowland et al., 2014). Thus, our findings extend previous observations that endothelial barriers differ in distinct CNS regions. A higher rate of TJ remodeling in the spinal cord vasculature may contribute to its increased vulnerability to EAE (Cruz-Orengo et al., 2014).

What regulates TJ remodeling during inflammation? Caveolae have been proposed to promote TJ endocytosis *in vitro* in CNS and non-CNS endothelial cells, as well as *in vivo* in non-CNS endothelial cells (Chang et al., 2009; Miyawaki-Shimizu et al., 2006; Rosengren et al., 2006; Schubert et al., 2002; Song et al., 2007). However, we find that *Cav1*$^{-/-}$ and wild-type mice exhibit similar kinetics of TJ remodeling and BSCB vascular leakage to small-molecular-weight tracers (e.g. biocytin-TMR) during EAE. These results extend our prior study that TJ remodeling is independent of caveolae during barrier breakdown following transient middle cerebral artery occlusion (t-MCAO), a mouse model for ischemic stroke (Knowland et al., 2014). Our data are consistent with caveolae- and clathrin-independent TJ remodeling/degradation in the CNS endothelium during EAE. A potential mechanism for TJ degradation could be enhanced endocytotic or macropinocytic remodeling/degradation in response to inflammatory cytokines such as IFN-γ (Bruewer et al., 2005). Thus, regulatory mechanisms underlying endothelial barrier integrity and dysfunction in CNS diseases differ from those proposed for epithelial barriers of the intestine and endothelial cells in the lung (Gunzel and Yu, 2013). The prevalence of dynamic protrusions at pre-clinical EAE (Fig. 1G,H,N) is consistent with the proposed role for neutrophils in promoting early BBB breakdown by secretion of proteolytic enzymes (Aube et al., 2014; Carlson et al., 2008). The lateral border recycling compartment can serve as the organelle where rapid remodeling of TJ proteins occurs in BECs *in vitro* as they encounter transmigrating monocytes (Winger et al., 2014). These organelles contain both AJ- and TJ-associated proteins, and may correspond to the TJ protrusions observed by two-photon imaging in gut epithelial cells (Marchiando et al., 2010) and BECs in the ischemic brain (Knowland et al., 2014) and spinal cord during inflammation (Fig. 1). Our finding that CFA/Ptx does not increase dynamic TJ protrusions at the BSCB (Fig. 1), or caveolar transcytosis of albumin (Fig. 4) suggest that it may prime BSCB TJs for endocytosis to facilitate EAE induction.

Our results also reveal a striking difference between the cell biological mechanisms of BBB disruption in EAE as compared to ischemic stroke. In t-MCAO, caveolar density and albumin uptake in cortical endothelium is enhanced as early as 6 h after reperfusion of an occluded vessel (Haley and Lawrence, 2017; Knowland et al., 2014). However, a high fraction of endothelial TJ protrusions and gaps associated with increased biocytin permeability are observed only 24–48 h after reperfusion (Haley and Lawrence, 2017; Knowland et al., 2014). Therefore, the mechanisms that safeguard the transcellular endothelial barrier fail before those that regulate the paracellular barrier in ischemic stroke (Haley and Lawrence, 2017; Knowland et al., 2014). In contrast, paracellular permeability is an early and persistent feature of EAE, whereas transcellular permeability is only elevated during severe disease stages (Figs. 3, 4 and S4C). This mechanistic dichotomy for barrier breakdown during t-MCAO versus EAE may be due to either distinct inflammatory triggers or the timing when leukocyte subsets infiltrate the CNS in these two disorders (Lopes Pinheiro et al., 2015).

Our analysis reveals a role for caveolae in selective trafficking of specific T cell subtypes across the BSCB. We find that mice lacking caveolae (Razani et al., 2001) are partially protected from EAE, demyelination and infiltration of INF-γ-producing Th1 subtypes into the spinal cord (Fig. 5). Our data are consistent with a recent study showing that *Cav1*$^{-/-}$ mice are protected from EAE pathology and entry of T cells (Wu et al., 2016). However, in contrast to that study, we find that the numbers of CD4^{+} and Th17^{+} lymphocytes that infiltrate the CNS are unchanged in *Cav1*$^{-/-}$ and wild-type EAE mice (Wu et al., 2016). This discrepancy may be due to inter-strain genetic or microbiome differences between mice used in both studies. Our study employed *Cav1*$^{-/-}$ mice on a C57BL/6J background, whereas Wu and colleagues used C57BL/6N (Wu et al., 2016). Since ~0.8% of genes differ between these substrains (Zurita et al., 2011), genetic heterogeneity may contribute to the reported differences. Commensal segmented filamentous bacteria (SFB), present in BL/6N, drives Th17 differentiation (Ivanov et al., 2009) and confers susceptibility to autoimmune arthritis in BL/6J by enhancing IL-17A production (Wu et al., 2010), a cytokine that disrupts TJs (Kebir et al., 2007). The gut microbiome regulates maturation of the BBB (Braniste et al., 2014) and changes the phenotypic manifestation of cerebral cavernous malformations, a CNS vascular disease, in the same genetic background (Tang et al., 2017). These factors could contribute to differences in the phenotype observed between two studies in *Cav1*$^{-/-}$ EAE mice.

Previous studies have indicated unique temporal profiles of Th1 and Th17 effector cell infiltration into the CNS. Th17 cells are highest in the EAE spinal cord at 7 days post-immunization and decrease to baseline by day 10, whereas Th1 cells are low at day 10 and escalate in the EAE spinal cord at day 14 (Murphy et al., 2010). Consistently, adoptive transfer of Th17 cells that are differentiated *ex vivo* induces more rapid clinical presentation of disease, as compared with adoptive transfer of Th1 cells differentiated *ex vivo* (Rothhammer et al., 2011). Our finding that Cav1 is not required for early TJ remodeling nor early development of clinical EAE is consistent with a caveolin-independent TJ remodeling driving Th17 infiltration and disease initiation, followed by caveolar transcytosis driving Th1 infiltration and disease propogation. Our tracer experiments support this idea. The TJ-permeant tracer biotin-TMR crosses the BBB at early/mild EAE, whereas the transcellular

substrate albumin crosses at later/severe disease. Fibrinogen promotes *de novo* caveolae formation in BECs (Muradashvili et al., 2014), and may contribute to enhanced transcellular permeability at severe EAE (Fig. 4). Importantly, our finding suggest that efforts to inhibit caveolar transcytosis hold therapeutic potential to counter neuroinflammation in MS patients.

Why do Th1 cells preferentially cross the BSCB via caveolae during EAE? Cell adhesion molecules such as ICAM-1/2 and VCAM-1 are enriched in caveolae and support transcellular migration by engaging infiltrating cell podocytes (Abadier et al., 2015; Carman and Martinelli, 2015; Millan et al., 2006). Th17 cells rely primarily on an αLβ2/ICAM-1 interaction (Rothhammer et al., 2011; Stromnes et al., 2008), whereas Th1 cells employ an α4/VCAM-1 complex for migration (Glatigny et al., 2011). Therefore, selective interactions between these adhesion molecules may direct Th1 cells more effectively toward caveolae when crossing the endothelium during neuroinflammation. We have recently shown that partial protection conferred by activation of Wnt/β-catenin signaling in the neurovasculature during EAE is associated with suppression of Caveolin-1, VCAM-1 and T cell infiltration (Lengfeld et al., 2017). Our findings therefore suggest that inhibiting both TJ degradation and caveolar transcytosis is a rationale for future therapies aimed at preventing immune cell entry into the CNS during autoimmune disease.

MATERIALS AND METHODS

Mice

All experimental procedures were approved by IACUC regulatory bodies at Columbia University Medical Center and the University of California, Irvine. Generation of *Tg eGFP-Claudin5*$^{+/-}$ has been described (Knowland et al., 2014). *Cav1*$^{-/-}$ mice (Razani et al., 2001) and *Rorc(γt)*$^{GFP/+}$ mice (Ivanov et al., 2006) were obtained from the Jackson Laboratories (Maine). All mice were backcrossed to the C57BL/6J strain (Jackson Laboratories) for more than 8 generations.

Experimental autoimmune encephalomyelitis induction

EAE was induced in 8-to 12 week-old female mice by subcutaneous immunization with 100 μl emulsion of 100 μg myelin oligodendrocyte glycoprotein ($MOG_{35–55}$) (MEVGWYRSPFSRVVHLYRNGK; ThermoFisher Scientific) in PBS with complete Freund's adjuvant (CFA) containing 200 μg *Mycobacterium tuberculosis* H37Ra (DIFCO). The day of MOG immunization was designated as day 0. Mice received intravenous injections of 400 ng *Bordetella pertussis* toxin (List Biological Laboratories) 0 and 2 days post-immunization (dpi). Control animals received *B. pertussis* toxin and emulsion containing PBS/CFA without MOG. Mice were examined for clinical EAE signs using the following scale, with 0.5-point gradations for intermediate presentation: 0, no signs; 1, flaccid tail; 2, hind limb paresis; 3, hind limb paralysis; 4, hind limb and forelimb paralysis; 5, moribund (Lutz et al., 2012).

Laminectomy and in vivo two-photon imaging

Mice were anesthetized with 2.5% isoflurane in O_2 and maintained throughout surgery and imaging at 1.5% isoflurane in O_2 supplemented with subcutaneous carprofen (5 mg/kg) and lactated Ringer's solution. Body temperature was maintained at 37.5°C using a feedback-controlled homeothermic heating pad. Lumbar level 1 (L1) vertebra was removed leaving the *dura mater* intact. A 3 mm borosilicate #0 coverslip was implanted on a bed of 1.5% agarose (in artificial cerebrospinal fluid) over the laminectomy site. The spinal column was stabilized using a custom-made titanium chamber affixed to adjacent vertebra with Vetbond and dental acrylic (Fig. 1A). Intravital imaging was performed on a two-photon microscope (Sutter MOM) with 920 nm excitation light (Mai Tai eHP Deep See; Spectra-Physics). Green fluorescence emission (Chroma 565 dcxr) was gathered using a 40X IR objective (Olympus, 0.8 NA). ScanImage software (Pologruto et al., 2003) was used to acquire 60–150 μm optical stacks beneath the dura, sampled in 0.5 μm or 1 μm steps axially. Acquisition of each stack lasted 2–3 minutes. Repeated time-lapse acquisition was performed at ~45-minute intervals. Capillaries were identified by morphology (i.e. less than 2 endothelial cells across, <10 μm). Arterioles and venules were differentiated by direction of blood flow (arteriole>capillary>venule>median vein) and endothelial cell morphology (arterioles with elongated shape, venules with cobblestone shape (Knowland et al., 2014)). Image dimensions were 204.8 μm × 204.8 μm (512 × 512 pixels).

TJ remodeling analysis

Images were analyzed with Fiji software (Schindelin et al., 2012) as described (Knowland et al., 2014). Optical slices in which the image was shifted by more than ~0.5 μm in the X or Y plane or ~1 μm in the Z plane due to motion artifacts were excised. TJ segments were defined as a continuous line between two endothelial cell borders without bifurcation. TJ segments were manually traced onto individual optical sections. TJ segments that were not visible at all time points were omitted from analysis. Protrusions were defined as eGFP-positive bulbous structures that extend >1 μm away from the long axis of a TJ segment (Fig. 1C, yellow arrow). Protrusions not present at both the beginning and end of the imaging session were considered dynamic (Fig. 1; red arrows). Gaps were defined as TJ segment discontinuities >0.4 μm (Fig. 1D). Tortuous strands were defined as TJ segments with multiple curvilinear sections departing >1 μm from the long axis (Fig. 1C). The number of protrusions, dynamic protrusions, gaps and tortuous segments were measured for each optical Z section.

BBB permeability *in vivo*

Thirty minutes after intravenous injection of 1% biocytin-TMR or albumin-AlexaFluor 594 (ThermoFisher Scientific), C57BL/6J, *Tg eGFP-Claudin5*$^{+/-}$*; Cav1*$^{-/-}$ or *Tg eGFP-Claudin5*$^{+/-}$ *Cav1*$^{-/-}$ mice were perfused with PBS and 4% paraformaldehyde (PFA). Tissues were post-fixed for 2–6 hours with 4% PFA, washed with PBS, cryoprotected in 30% sucrose overnight, embedded in OCT, sectioned and immunostained for Glut-1 (Calbiochem; 1:2000) to visualize blood vessels, fibrinogen (LifeSpan Biosciences 1:4000) for leakage across the BBB and streptavidin-AlexaFluor 594 (ThermoFisher Scientific; 1:2000) to visualize biocytin-TMR tissue distribution. Sections were imaged with a Zeiss

LSM700 confocal microscope. Biocytin-TMR leakage was quantified as described (Knowland et al., 2014), by measuring the mean fluorescence intensity in spinal cord sections, and presented as ratios to mean fluorescence intensities in liver sections. Three to six sections at thoracic and three to six sections at lumbar spinal cord levels were quantified and averaged for each mouse. No significant differences in biocytin-TMR intensity within the liver were noted among groups. Fibrinogen-positive pixels were measured and divided by the area of the spinal cord section. Albumin-AlexaFluor 594 uptake was measured as described (Knowland et al., 2014). Albumin-AlexaFluor 594 single-channel images were uniformly thresholded and pixels above the threshold were counted both within (endothelial-associated albumin) and outside of endothelial cells (parenchyma-associated albumin; Fig. 4).

T cell differentiation and transmigration *in vitro*

For Th1 cultures, splenocytes from C57BL/6 mice were collected 6 days after MOG-immunization and cultured in Th1-polarizing conditions in the presence of antigen [20 μg/ml MOG plus 1 ng/ml IL-12, in RPMI supplemented with FBS, L-glutamine, beta-mercaptoethanol and non-essential amino acids (Murphy et al., 2010)]. After 4 days, 5 ng/ml IL-2 was added (Murphy et al., 2010). After 7 days in culture, production of the Th1 cytokine IFN-γ increased ~4000% (Fig. S5C and data not shown). For Th17 cultures, splenocytes from *Rorc(γt)*$^{GFP/+}$ (Ivanov et al., 2006) were collected 6 days after MOG-immunization and cultured in Th17-polarizing conditions with antigen: 20 μg/ml MOG, 10 ng/ml IL-1β, 30 ng/ml IL-6, 3 ng/ml TGF-β, 10 μg/ml anti-IFN-γ, 10 μg/ml anti-IL-4. After 4 days, 20 ng/ml IL-23 was added. After 3 additional days, cells were re-stimulated with 0.5 μg/ml plate-bound anti-CD3 and 0.5 μg/ml soluble anti-CD28 (Cravens et al., 2016). Th17 cultures had ~4000-fold increased production of IL-17 (Fig. S5C). Th1 or Th17 cultures were applied to monolayers of primary mouse brain microvascular endothelial cells from WT or *Cav1*$^{-/-}$ mice (Cell Biologics, Inc.) grown on Collagen IV-coated glass-bottom plates in the presence of shear forces (10 dyn/cm^2 orbital rotation) and activated overnight with 1 ng/ml TNF-α (Martinelli et al., 2014). In some experiments brain endothelial cells were pretreated for 2h with caveolae inhibitors genistein (Sigma, 400 μM), methyl-β-cyclodextrin (Sigma, 5 mM), or vehicle (OptiMEM, Gibco). T cells were allowed to adhere and transmigrate for 90 minutes at 37°C, washed 5X with warm HBSS, fixed with 4% PFA and immunostained with anti-CD4 or CD45, anti-ZO-1, anti-GFP, and DAPI. An LSM700 confocal microscope equipped with a 40X water-immersion objective was used to determine positions of cells as superficial (adherent) or transmigratory (Martinelli et al., 2014). At least 50 cells/group were quantified across 6 wells per condition, in three independent experiments.

Immunofluorescence and antibodies

Rabbit anti-Caveolin1 (Calbiochem 1:4000), rat anti-CD4 (BD Pharmingen clone RM4–5, 1:100), rabbit anti-CD45 (Sigma 1:250), rabbit anti-GFP (1:1000), mouse anti-ZO-1 (Invitrogen 1:1000), mouse anti-CC1 (Santa Cruz 1:200), rabbit anti-cleaved Caspase 3 (Cell Signaling 1:250), rabbit anti-Fibrinogen (LifeSpan Biosciences 1:4000), rabbit anti-Glut1 (Calbiochem 1:2000) and rabbit anti-Laminin (Sigma 1:4000). Cells immunoreactive for CD4 inside the CNS parenchyma, and in meningeal and intraluminal spaces (delineated by

laminin staining), were counted for six to eight thoracic spinal cord sections from each mouse. For unbiased measurement of myelinated areas, Fiji software was used to measure fluoromyelin-positive pixels (ThermoFisher Scientific; 1:300) in uniformly thresholded images, and expressed as a ratio of total white matter area.

Flow cytometry

Spinal cords from wild-type and *Cav1*$^{-/-}$ mice 15 dpi were homogenized between frosted glass slides. Mononuclear cells were isolated at the interphase of a 30–70% Percoll gradient (GE Healthcare). Draining lymph nodes and spleens were mechanically homogenized and red blood cells lysed. Single cell suspensions were re-stimulated for 5 hours *in vitro* with phorbol 12-myristate 13-acetate (PMA), ionomycin, brefeldin and monensin (eBioscience). After F_c receptor blockade, cells were stained with Live-Dead Aqua (Invitrogen) plus antibodies against CD4-BV605 (BD Pharmingen), CD8-PECy5 (Biolegend), CD45-BV421 (BD Pharmingen) and CD19-PECy7 (BD Pharmingen). Cells were then fixed, permeabilized and stained for IL-17a-PE (BD Pharmingen) and IFN-γ-APC (BD Pharmingen). Unstained CNS mononuclear cells were used for single-channel compensation, isotype controls and fluorescence-minus-one controls.

Statistical analysis

We performed two-way t-tests for pairwise comparisons and one-way ANOVA followed by Newman-Keul's multiple comparison tests for group effects. EAE was assessed by two-way repeated measure ANOVA followed by Sidak's multiple comparison test. EAE was analyzed in 34 wild-type and 32 *Cav1*$^{-/-}$ mice. Mice with no clinical disease presentation were included in the analysis (1 wild-type and 2 *Cav1*$^{-/-}$), and animals that died during the experiment were excluded from analysis (no wild-type and 2 *Cav1*$^{-/-}$). Statistical analyses were performed with GraphPad Prism software, and statistical significance for all figures is displayed as NS, $p>0.05$, *$p<0.05$, **$p<0.01$ and ***$p<0.001$.

Supplementary Material

Refer to Web version on PubMed Central for supplementary material.

Acknowledgments

We thank Tyler Cutforth, Celia F. Brosnan and Cedric S. Raine for scientific and editorial input, Ilir Agalliu for statistical advice and Adeela Syed from the UC Irvine Optical Biology Core for use of the LSM700 confocal microscope. S.E.L., J.R.S. and D.A. were supported the NIH (#R01 HL116995, #R56 MH109987 and #R01 MH112849), the National Multiple Sclerosis Society (NMSS #RG4673A1/1 and #FG2035-A-1), the Leducq Foundation (D.A.) and an unrestricted gift from John Castle to the Department of Neurology, Stroke Division at CUMC (D.A.). D.H.K. and C.V.L.O. were supported by UC Irvine Undergraduate Research Opportunity (UROP) fellowships. S.P.G. was supported by a Searle Scholar Award, a Klingenstein fellowship and an NMSS grant (#RG4673A1/1). The Optical Biology Shared Resource of UC Irvine is funded by a Cancer Center support grant (#CA-62203). The Columbia University Medical Center CCTI Flow Cytometry Core is supported in part by the Office of the Director, NIH (#S10RR027050). The funders had no role in study design, data collection and analysis, decision to publish nor preparation of the manuscript. The authors declare no competing financial interests.

NON-STANDARD ABBREVIATIONS AND ACRONYMS

BBB blood-brain barrier

BSCB	blood-spinal cord barrier
BEC	brain endothelial cell
Cav1	Caveolin1
CFA	complete Freund's adjuvant
CNS	central nervous system
EAE	experimental autoimmune encephalomyelitis
EC	endothelial cell
eGFP	enhanced green fluorescent protein
MOG	myelin oligodendrocyte glycoprotein
MS	multiple sclerosis
Ptx	*B. pertussis* toxin
L1	lumbar level 1
Tg	transgenic
TJ	tight junction

References

Abadier M, Haghayegh Jahromi N, Cardoso Alves L, Boscacci R, Vestweber D, Barnum S, Deutsch U, Engelhardt B, Lyck R. Cell surface levels of endothelial ICAM-1 influence the transcellular or paracellular T-cell diapedesis across the blood-brain barrier. Eur J Immunol. 2015; 45:1043–1058. [PubMed: 25545837]

Al-Izki S, Pryce G, O'Neill JK, Butter C, Giovannoni G, Amor S, Baker D. Practical guide to the induction of relapsing progressive experimental autoimmune encephalomyelitis in the Biozzi ABH mouse. Multiple sclerosis and related disorders. 2012; 1:29–38. [PubMed: 25876448]

Alvarez JI, Saint-Laurent O, Godschalk A, Terouz S, Briels C, Larouche S, Bourbonniere L, Larochelle C, Prat A. Focal disturbances in the blood-brain barrier are associated with formation of neuroinflammatory lesions. Neurobiology of disease. 2015; 74:14–24. [PubMed: 25448765]

Aube B, Levesque SA, Pare A, Chamma E, Kebir H, Gorina R, Lecuyer MA, Alvarez JI, De Koninck Y, Engelhardt B, et al. Neutrophils mediate blood-spinal cord barrier disruption in demyelinating neuroinflammatory diseases. Journal of immunology (Baltimore, Md: 1950). 2014; 193:2438–2454.

Bartanusz V, Jezova D, Alajajian B, Digicaylioglu M. The blood-spinal cord barrier: morphology and clinical implications. Annals of neurology. 2011; 70:194–206. [PubMed: 21674586]

Bennett J, Basivireddy J, Kollar A, Biron KE, Reickmann P, Jefferies WA, McQuaid S. Blood-brain barrier disruption and enhanced vascular permeability in the multiple sclerosis model EAE. Journal of neuroimmunology. 2010; 229:180–191. [PubMed: 20832870]

Braniste V, Al-Asmakh M, Kowal C, Anuar F, Abbaspour A, Toth M, Korecka A, Bakocevic N, Ng LG, Kundu P, et al. The gut microbiota influences blood-brain barrier permeability in mice. Sci Transl Med. 2014; 6:263ra158.

Brown WJ. The capillaries in acute and subacute multiple sclerosis plaques: a morphometric analysis. Neurology. 1978; 28:84–92. [PubMed: 568753]

Bruewer M, Utech M, Ivanov AI, Hopkins AM, Parkos CA, Nusrat A. Interferon-gamma induces internalization of epithelial tight junction proteins via a macropinocytosis-like process. FASEB

journal: official publication of the Federation of American Societies for Experimental Biology. 2005; 19:923–933. [PubMed: 15923402]

Carlson T, Kroenke M, Rao P, Lane TE, Segal B. The Th17-ELR+ CXC chemokine pathway is essential for the development of central nervous system autoimmune disease. The Journal of experimental medicine. 2008; 205:811–823. [PubMed: 18347102]

Carman CV, Martinelli R. T Lymphocyte-Endothelial Interactions: Emerging Understanding of Trafficking and Antigen-Specific Immunity. Frontiers in immunology. 2015; 6:603. [PubMed: 26635815]

Chang SH, Feng D, Nagy JA, Sciuto TE, Dvorak AM, Dvorak HF. Vascular permeability and pathological angiogenesis in caveolin-1-null mice. The American journal of pathology. 2009; 175:1768–1776. [PubMed: 19729487]

Cheng JP, Nichols BJ. Caveolae: One Function or Many? Trends in cell biology. 2016; 26:177–189. [PubMed: 26653791]

Claudio L, Brosnan CF. Effects of prazosin on the blood-brain barrier during experimental autoimmune encephalomyelitis. Brain Res. 1992; 594:233–243. [PubMed: 1450949]

Cravens PD, Hussain RZ, Miller-Little WA, Ben LH, Segal BM, Herndon E, Stuve O. IL-12/IL-23p40 Is Highly Expressed in Secondary Lymphoid Organs and the CNS during All Stages of EAE, but Its Deletion Does Not Affect Disease Perpetuation. PloS one. 2016; 11:e0165248. [PubMed: 27780253]

Cruz-Orengo L, Daniels BP, Dorsey D, Basak SA, Grajales-Reyes JG, McCandless EE, Piccio L, Schmidt RE, Cross AH, Crosby SD, et al. Enhanced sphingosine-1-phosphate receptor 2 expression underlies female CNS autoimmunity susceptibility. J Clin Invest. 2014; 124:2571–2584. [PubMed: 24812668]

Daneman R, Engelhardt B. Brain barriers in health and disease. Neurobiology of disease. 2017; 107:1–3. [PubMed: 28552387]

Dileepan T, Smith ED, Knowland D, Hsu M, Platt M, Bittner-Eddy P, Cohen B, Southern P, Latimer E, Harley E, et al. Group A Streptococcus intranasal infection promotes CNS infiltration by streptococcal-specific Th17 cells. J Clin Invest. 2016; 126:303–317. [PubMed: 26657857]

Engelhardt B, Wolburg H. Mini-review: Transendothelial migration of leukocytes: through the front door or around the side of the house? Eur J Immunol. 2004; 34:2955–2963. [PubMed: 15376193]

Fabis MJ, Phares TW, Kean RB, Koprowski H, Hooper DC. Blood-brain barrier changes and cell invasion differ between therapeutic immune clearance of neurotrophic virus and CNS autoimmunity. Proceedings of the National Academy of Sciences of the United States of America. 2008; 105:15511–15516. [PubMed: 18829442]

Glatigny S, Duhen R, Oukka M, Bettelli E. Cutting edge: loss of alpha4 integrin expression differentially affects the homing of Th1 and Th17 cells. Journal of immunology (Baltimore, Md: 1950). 2011; 187:6176–6179.

Gunzel D, Yu AS. Claudins and the modulation of tight junction permeability. Physiological reviews. 2013; 93:525–569. [PubMed: 23589827]

Haley MJ, Lawrence CB. The blood-brain barrier after stroke: Structural studies and the role of transcytotic vesicles. Journal of cerebral blood flow and metabolism: official journal of the International Society of Cerebral Blood Flow and Metabolism. 2017; 37:456–470.

Ivanov II, Atarashi K, Manel N, Brodie EL, Shima T, Karaoz U, Wei D, Goldfarb KC, Santee CA, Lynch SV, et al. Induction of intestinal Th17 cells by segmented filamentous bacteria. Cell. 2009; 139:485–498. [PubMed: 19836068]

Ivanov II, McKenzie BS, Zhou L, Tadokoro CE, Lepelley A, Lafaille JJ, Cua DJ, Littman DR. The orphan nuclear receptor RORgammat directs the differentiation program of proinflammatory IL-17+ T helper cells. Cell. 2006; 126:1121–1133. [PubMed: 16990136]

Kebir H, Kreymborg K, Ifergan I, Dodelet-Devillers A, Cayrol R, Bernard M, Giuliani F, Arbour N, Becher B, Prat A. Human TH17 lymphocytes promote blood-brain barrier disruption and central nervous system inflammation. Nature medicine. 2007; 13:1173–1175.

Kirk J, Plumb J, Mirakhur M, McQuaid S. Tight junctional abnormality in multiple sclerosis white matter affects all calibres of vessel and is associated with blood-brain barrier leakage and active demyelination. J Pathol. 2003; 201:319–327. [PubMed: 14517850]

Knowland D, Arac A, Sekiguchi KJ, Hsu M, Lutz SE, Perrino J, Steinberg GK, Barres BA, Nimmerjahn A, Agalliu D. Stepwise recruitment of transcellular and paracellular pathways underlies blood-brain barrier breakdown in stroke. Neuron. 2014; 82:1–15. [PubMed: 24698262]

Komarova YA, Kruse K, Mehta D, Malik AB. Protein Interactions at Endothelial Junctions and Signaling Mechanisms Regulating Endothelial Permeability. Circulation research. 2017; 120:179–206. [PubMed: 28057793]

Kovtun O, Tillu VA, Ariotti N, Parton RG, Collins BM. Cavin family proteins and the assembly of caveolae. Journal of cell science. 2015; 128:1269–1278. [PubMed: 25829513]

Lampugnani MG, Bravi L, Dejana E. The role of microvascular endothelial WNT signaling the formation of the blood brain barrier. SpringerPlus. 2015; 4:L47. [PubMed: 27386209]

Lengfeld JE, Lutz SE, Smith JR, Diaconu C, Scott C, Kofman SB, Choi C, Walsh CM, Raine CS, Agalliu I, et al. Endothelial Wnt/beta-catenin signaling reduces immune cell infiltration in multiple sclerosis. Proceedings of the National Academy of Sciences of the United States of America. 2017

Lopes Pinheiro MA, Kooij G, Mizee MR, Kamermans A, Enzmann G, Lyck R, Schwaninger M, Engelhardt B, de Vries HE. Immune cell trafficking across the barriers of the central nervous system in multiple sclerosis and stroke. Biochim Biophys Acta. 2015

Louveau A, Plog BA, Antila S, Alitalo K, Nedergaard M, Kipnis J. Understanding the functions and relationships of the glymphatic system and meningeal lymphatics. J Clin Invest. 2017; 127:3210–3219. [PubMed: 28862640]

Lutz SE, Raine CS, Brosnan CF. Loss of astrocyte connexins 43 and 30 does not significantly alter susceptibility or severity of acute experimental autoimmune encephalomyelitis in mice. Journal of neuroimmunology. 2012; 245:8–14. [PubMed: 22342190]

Marchiando AM, Shen L, Graham WV, Weber CR, Schwarz BT, Austin JR 2nd, Raleigh DR, Guan Y, Watson AJ, Montrose MH, et al. Caveolin-1-dependent occludin endocytosis is required for TNF-induced tight junction regulation in vivo. J Cell Biol. 2010; 189:111–126. [PubMed: 20351069]

Martinelli R, Zeiger AS, Whitfield M, Sciuto TE, Dvorak A, Van Vliet KJ, Greenwood J, Carman CV. Probing the biomechanical contribution of the endothelium to lymphocyte migration: diapedesis by the path of least resistance. Journal of cell science. 2014; 127:3720–3734. [PubMed: 25002404]

Millan J, Hewlett L, Glyn M, Toomre D, Clark P, Ridley AJ. Lymphocyte transcellular migration occurs through recruitment of endothelial ICAM-1 to caveola-and F-actin-rich domains. Nat Cell Biol. 2006; 8:113–123. [PubMed: 16429128]

Miyawaki-Shimizu K, Predescu D, Shimizu J, Broman M, Predescu S, Malik AB. siRNA-induced caveolin-1 knockdown in mice increases lung vascular permeability via the junctional pathway. Am J Physiol Lung Cell Mol Physiol. 2006; 290:L405–413. [PubMed: 16183667]

Muradashvili N, Khundmiri SJ, Tyagi R, Gartung A, Dean WL, Lee MJ, Lominadze D. Sphingolipids affect fibrinogen-induced caveolar transcytosis and cerebrovascular permeability. American journal of physiology Cell physiology. 2014; 307:C169–179. [PubMed: 24829496]

Murphy AC, Lalor SJ, Lynch MA, Mills KH. Infiltration of Th1 and Th17 cells and activation of microglia in the CNS during the course of experimental autoimmune encephalomyelitis. Brain, behavior, and immunity. 2010; 24:641–651.

Nag S. Ultracytochemical studies of the compromised blood-brain barrier. Methods Mol Med. 2003; 89:145–160. [PubMed: 12958418]

Nitta T, Hata M, Gotoh S, Seo Y, Sasaki H, Hashimoto N, Furuse M, Tsukita S. Size-selective loosening of the blood-brain barrier in claudin-5-deficient mice. J Cell Biol. 2003; 161:653–660. [PubMed: 12743111]

Paul D, Cowan AE, Ge S, Pachter JS. Novel 3D analysis of Claudin-5 reveals significant endothelial heterogeneity among CNS microvessels. Microvascular research. 2013; 86:1–10. [PubMed: 23261753]

Pfeiffer F, Schafer J, Lyck R, Makrides V, Brunner S, Schaeren-Wiemers N, Deutsch U, Engelhardt B. Claudin-1 induced sealing of blood-brain barrier tight junctions ameliorates chronic experimental autoimmune encephalomyelitis. Acta neuropathologica. 2011; 122:601–614. [PubMed: 21983942]

Platt MP, Agalliu D, Cutforth T. Hello from the Other Side: How Autoantibodies Circumvent the Blood-Brain Barrier in Autoimmune Encephalitis. Frontiers in immunology. 2017; 8:442. [PubMed: 28484451]

Raine CS, Cannella B, Duijvestijn AM, Cross AH. Homing to central nervous system vasculature by antigen-specific lymphocytes. II. Lymphocyte/endothelial cell adhesion during the initial stages of autoimmune demyelination. Lab Invest. 1990; 63:476–489. [PubMed: 1700193]

Razani B, Engelman JA, Wang XB, Schubert W, Zhang XL, Marks CB, Macaluso F, Russell RG, Li M, Pestell RG, et al. Caveolin-1 null mice are viable but show evidence of hyperproliferative and vascular abnormalities. The Journal of biological chemistry. 2001; 276:38121–38138. [PubMed: 11457855]

Reese TS, Karnovsky MJ. Fine structural localization of a blood-brain barrier to exogenous peroxidase. J Cell Biol. 1967; 34:207–217. [PubMed: 6033532]

Reijerkerk A, Kooij G, van der Pol SM, Leyen T, van Het Hof B, Couraud PO, Vivien D, Dijkstra CD, de Vries HE. Tissue-type plasminogen activator is a regulator of monocyte diapedesis through the brain endothelial barrier. Journal of immunology (Baltimore, Md: 1950). 2008; 181:3567–3574.

Rosengren BI, Rippe A, Rippe C, Venturoli D, Sward K, Rippe B. Transvascular protein transport in mice lacking endothelial caveolae. Am J Physiol Heart Circ Physiol. 2006; 291:H1371–1377. [PubMed: 16501011]

Rostami A, Ciric B. Role of Th17 cells in the pathogenesis of CNS inflammatory demyelination. Journal of the neurological sciences. 2013; 333:76–87. [PubMed: 23578791]

Rothhammer V, Heink S, Petermann F, Srivastava R, Claussen MC, Hemmer B, Korn T. Th17 lymphocytes traffic to the central nervous system independently of alpha4 integrin expression during EAE. The Journal of experimental medicine. 2011; 208:2465–2476. [PubMed: 22025301]

Ryu JK, Petersen MA, Murray SG, Baeten KM, Meyer-Franke A, Chan JP, Vagena E, Bedard C, Machado MR, Coronado PE, et al. Blood coagulation protein fibrinogen promotes autoimmunity and demyelination via chemokine release and antigen presentation. Nat Commun. 2015; 6:8164. [PubMed: 26353940]

Santizo RA, Xu HL, Galea E, Muyskens S, Baughman VL, Pelligrino DA. Combined endothelial nitric oxide synthase upregulation and caveolin-1 downregulation decrease leukocyte adhesion in pial venules of ovariectomized female rats. Stroke. 2002; 33:613–616. [PubMed: 11823678]

Schubert W, Frank PG, Woodman SE, Hyogo H, Cohen DE, Chow CW, Lisanti MP. Microvascular hyperpermeability in caveolin-1 (−/−) knock-out mice. Treatment with a specific nitric-oxide synthase inhibitor, L-NAME, restores normal microvascular permeability in Cav-1 null mice. The Journal of biological chemistry. 2002; 277:40091–40098. [PubMed: 12167625]

Shin T, Kim H, Jin JK, Moon C, Ahn M, Tanuma N, Matsumoto Y. Expression of caveolin-1, -2, and -3 in the spinal cords of Lewis rats with experimental autoimmune encephalomyelitis. Journal of neuroimmunology. 2005; 165:11–20. [PubMed: 15925413]

Simmons SB, Liggitt D, Goverman JM. Cytokine-regulated neutrophil recruitment is required for brain but not spinal cord inflammation during experimental autoimmune encephalomyelitis. Journal of immunology (Baltimore, Md: 1950). 2014; 193:555–563.

Song L, Ge S, Pachter JS. Caveolin-1 regulates expression of junction-associated proteins in brain microvascular endothelial cells. Blood. 2007; 109:1515–1523. [PubMed: 17023578]

Stamatovic SM, Keep RF, Wang MM, Jankovic I, Andjelkovic AV. Caveolae-mediated internalization of occludin and claudin-5 during CCL2-induced tight junction remodeling in brain endothelial cells. The Journal of biological chemistry. 2009; 284:19053–19066. [PubMed: 19423710]

Stromnes IM, Cerretti LM, Liggitt D, Harris RA, Goverman JM. Differential regulation of central nervous system autoimmunity by T(H)1 and T(H)17 cells. Nature medicine. 2008; 14:337–342.

Sun Y, Hu G, Zhang X, Minshall RD. Phosphorylation of caveolin-1 regulates oxidant-induced pulmonary vascular permeability via paracellular and transcellular pathways. Circulation research. 2009; 105:676–685. [PubMed: 19713536]

Tang AT, Choi JP, Kotzin JJ, Yang Y, Hong CC, Hobson N, Girard R, Zeineddine HA, Lightle R, Moore T, et al. Endothelial TLR4 and the microbiome drive cerebral cavernous malformations. Nature. 2017; 545:305–310. [PubMed: 28489816]

Tiruppathi C, Song W, Bergenfeldt M, Sass P, Malik AB. Gp60 activation mediates albumin transcytosis in endothelial cells by tyrosine kinase-dependent pathway. The Journal of biological chemistry. 1997; 272:25968–25975. [PubMed: 9325331]

Tonra JR, Reiseter BS, Kolbeck R, Nagashima K, Robertson R, Keyt B, Lindsay RM. Comparison of the timing of acute blood-brain barrier breakdown to rabbit immunoglobulin G in the cerebellum and spinal cord of mice with experimental autoimmune encephalomyelitis. J Comp Neurol. 2001; 430:131–144. [PubMed: 11135250]

Umeda K, Ikenouchi J, Katahira-Tayama S, Furuse K, Sasaki H, Nakayama M, Matsui T, Tsukita S, Furuse M, Tsukita S. ZO-1 and ZO-2 independently determine where claudins are polymerized in tight-junction strand formation. Cell. 2006; 126:741–754. [PubMed: 16923393]

Winger RC, Koblinski JE, Kanda T, Ransohoff RM, Muller WA. Rapid remodeling of tight junctions during paracellular diapedesis in a human model of the blood-brain barrier. Journal of immunology (Baltimore, Md: 1950). 2014; 193:2427–2437.

Wu H, Deng R, Chen X, Wong WC, Chen H, Gao L, Nie Y, Wu W, Shen J. Caveolin-1 Is Critical for Lymphocyte Trafficking into Central Nervous System during Experimental Autoimmune Encephalomyelitis. The Journal of neuroscience: the official journal of the Society for Neuroscience. 2016; 36:5193–5199. [PubMed: 27170118]

Wu HJ, Ivanov II, Darce J, Hattori K, Shima T, Umesaki Y, Littman DR, Benoist C, Mathis D. Gut-residing segmented filamentous bacteria drive autoimmune arthritis via T helper 17 cells. Immunity. 2010; 32:815–827. [PubMed: 20620945]

Zurita E, Chagoyen M, Cantero M, Alonso R, Gonzalez-Neira A, Lopez-Jimenez A, Lopez-Moreno JA, Landel CP, Benitez J, Pazos F, et al. Genetic polymorphisms among C57BL/6 mouse inbred strains. Transgenic research. 2011; 20:481–489. [PubMed: 20506040]

HIGHLIGHTS

- Intravital two-photon microscopy shows that TJ remodeling precedes the onset of EAE.
- Caveolar transcytosis is not required for endothelial TJ remodeling *in vivo.*
- Effector T cell subsets use distinct mechanisms to cross the inflamed BBB.
- Caveolar transcytosis is required for Th1 but not Th17 cell entry into the CNS.

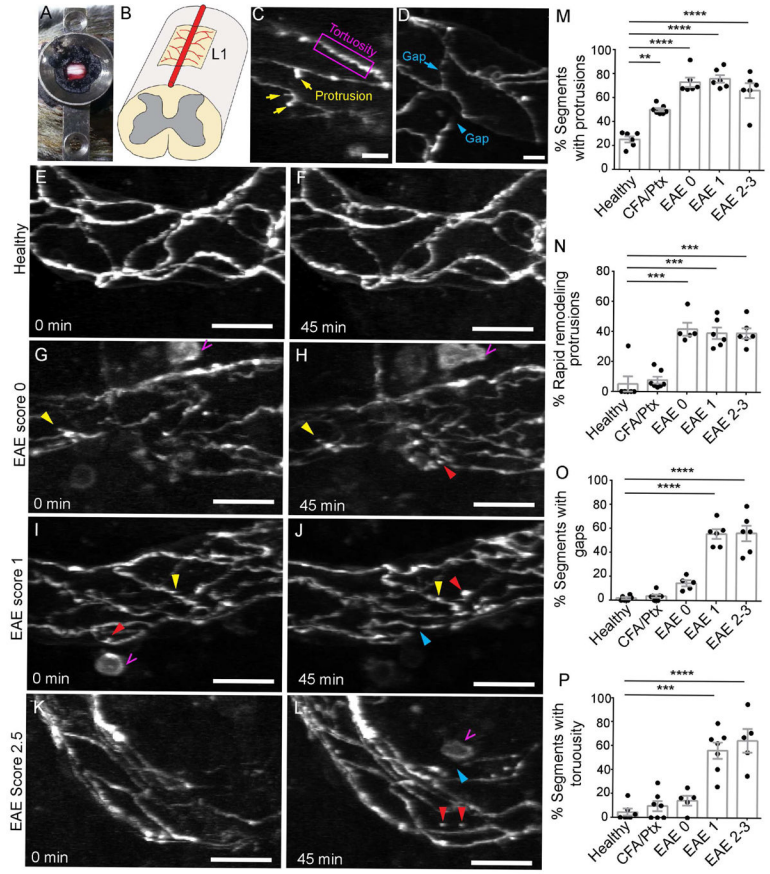

Figure 1. Dynamic tight junction changes in spinal cord blood vessels during EAE revealed by intravital two-photon microscopy of *Tg eGFP-Claudin5*$^{+/-}$ mice

A) Dorsal laminectomy and B) diagram of the imaging window in the dorsal white matter of lumbar level 1 (L1) spinal cord in mice. C–D) Examples of eGFP-positive tight junction (TJ) protrusions, tortuosity, and gaps. E–L) Maximum intensity projections of two sequential time-lapse images of spinal cord venules in healthy (E,F, n = 6), pre-clinical (G,H, n = 5, EAE score 0), mild EAE (I,J, n = 6, score 1) and severe EAE (K,L, n = 6, scores 2–3) *Tg eGFP-Claudin5*$^{+/-}$ mice at 0 and ~45-minute intervals. Yellow arrows show static TJ protrusions, red arrows point to dynamic TJ protrusions that appear or disappear during the imaging period, blue arrows show TJ gaps and magenta open arrows point to hematopoietic cells. (M–P) Bar graphs show percentages of TJ segments with protrusions (M), dynamic protrusions (N), gaps (O), and tortuosity (P). Each dot represents the mean of multiple fields from a single mouse. Bar graphs show mean ± SEM, *p<0.05, **p<0.01, ***p<0.001, one-way ANOVA. Scale bars are 20 μm (C,E–L) and 10 μm (D). See also Figure S1.

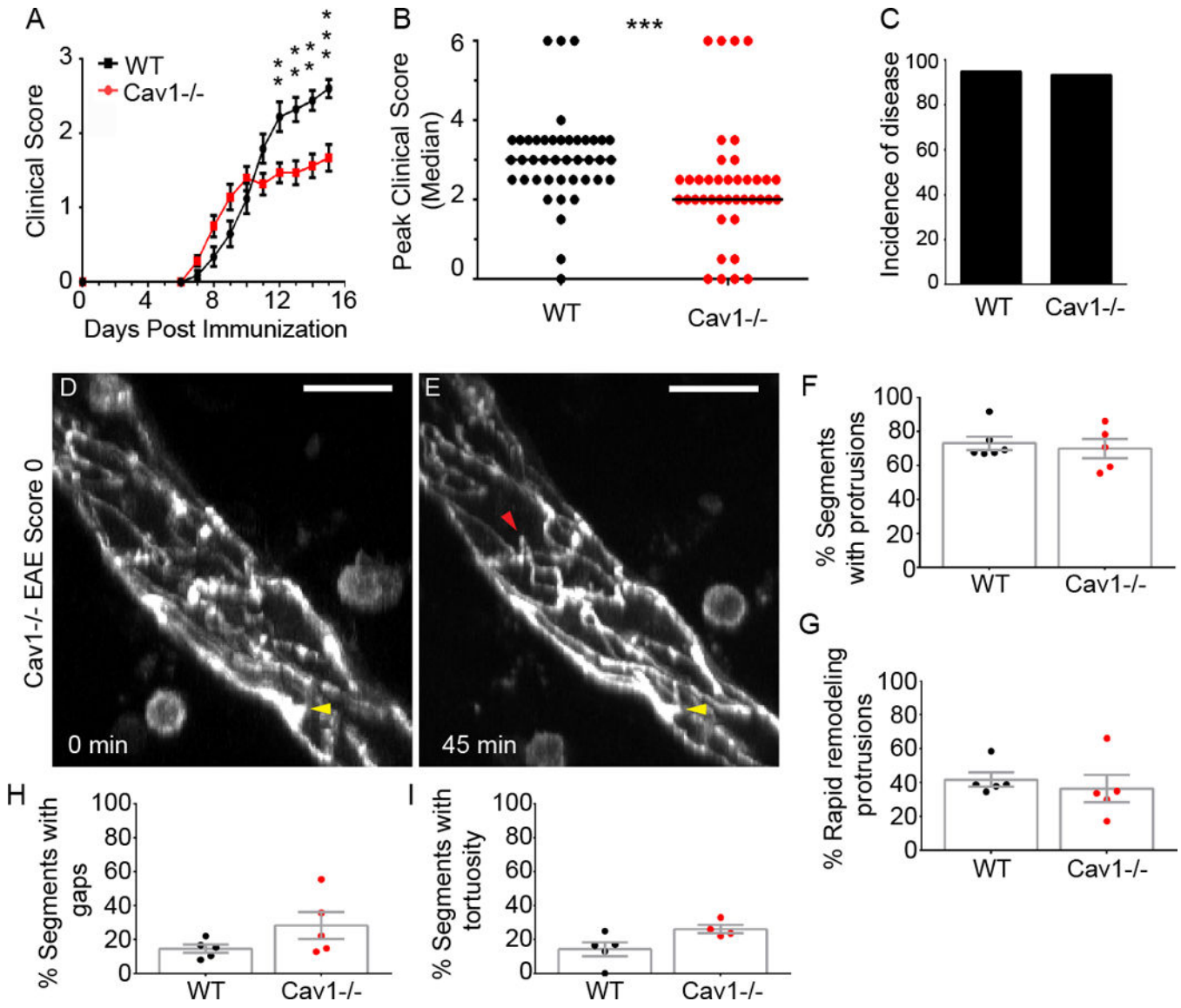

Figure 2. *Cav1*-deficient mice display attenuated EAE but no changes in TJ remodeling

A) Clinical EAE scores in wild-type (n = 34) and *Cav1*$^{-/-}$ (n = 32) littermate mice. *Cav1*$^{-/-}$ mice have less severe clinical scores at the indicated times [12–15 dpi, **p<0.01; ***p<0.001; two-way repeated measure ANOVA]. The graph excludes mice that died during the experiment (n = 0 wild-type, n = 2 *Cav1*$^{-/-}$). B) Scatter plot of maximum clinical scores attained by each mouse. *Cav1*$^{-/-}$ mice had less severe scores (p<0.001, Mann-Whitney comparison of medians). C) Bar graph of disease incidence. D–E) Maximum intensity projections of time-lapse imaging recordings (45 minutes) for spinal cord venules in *Tg eGFP-Claudin5*$^{+/-}$, *Cav1*$^{-/-}$ mice at EAE score 0 (n=5–6 group). Yellow arrows show static protrusions and red arrows point to dynamic protrusions that appear or disappear during the imaging period. Scale bars are 20 μm. F–I) Bar graphs show percentages of TJ segments with protrusions (F), dynamic protrusions (G), gaps (H), and tortuosity (I) between *Tg eGFP-Claudin5*$^{+/-}$, *and Tg eGFP-Claudin5*$^{+/-}$, *Cav1*$^{-/-}$ mice. No differences were found for

TJ structural features between *Tg eGFP-Claudin5*$^{+/-}$ and *Tg eGFP-Claudin5*$^{+/-}$*, Cav1*$^{-/-}$ mice. See also Figure S2.

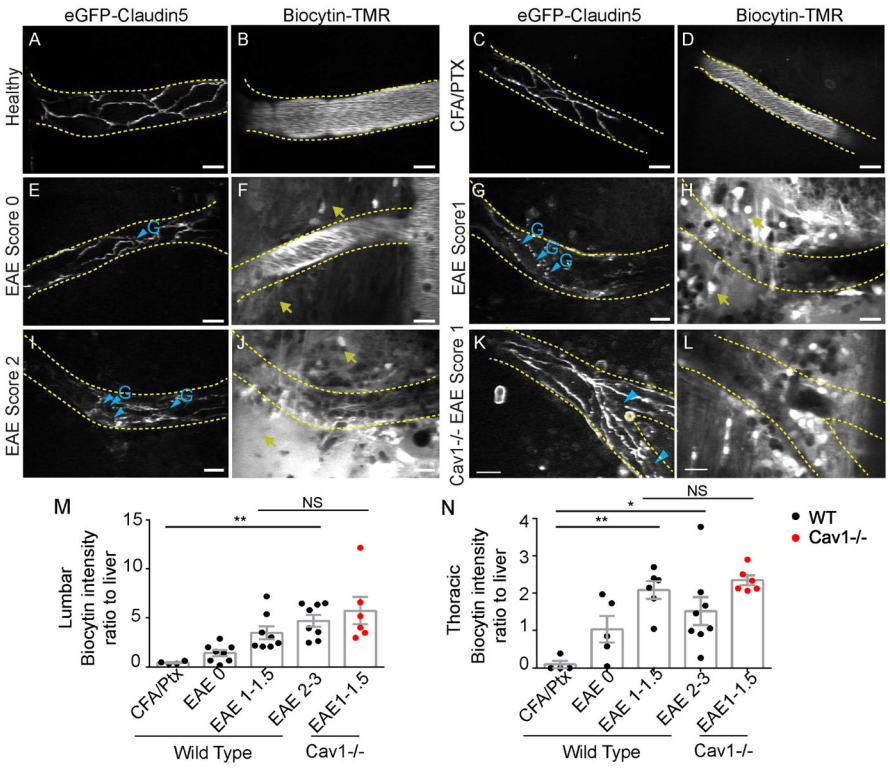

Figure 3. Paracellular BBB leakage in spinal cord blood vessels

Biocytin-TMR was intravenously injected into *Tg eGFP-Claudin5*$^{+/-}$ and *Tg eGFP-Claudin5*$^{+/-}$, *Cav1*$^{-/-}$ mice prior to *in vivo* imaging with two-photon microscopy. (A–D) Healthy and CFA/pertussis toxin control *Tg eGFP-Claudin-5*$^{+/-}$ mice had continuous TJ segments (A,C) and biocytin-TMR was confined within the lumen of spinal cord blood vessels (B,D). (E,F) *Tg eGFP-Claudin5*$^{+/-}$ mice with EAE score 0 had some TJ gaps (E; blue arrowheads) and minimal biocytin-TMR leakage outside of blood vessels (F; yellow arrows). (G–J) *Tg eGFP-Claudin5*$^{+/-}$ mice with EAE scores 1 (G–H) and 2 (I–J) had multiple TJ gaps (G,I; blue arrowheads) and extensive extravascular biocytin-TMR in the spinal cord (H,J; yellow arrows). (K–L) *Tg eGFP-Claudin5*$^{+/-}$, *Cav-1*$^{-/-}$ mice with EAE score 1 had multiple TJ gaps (blue arrowheads) and extravascular biocytin-TMR. (M–N) Graphs of biocytin-TMR fluorescence intensity in the lumbar (M) and thoracic (N) spinal cord normalized to fluorescence intensity in the liver *ex vivo* (n = 4 CFA/pertussis toxin control, n = 7 EAE score 0, n = 6 EAE score 1, n = 8 EAE score 2–3). Scale bars are 20 μm. See also Figure S3.

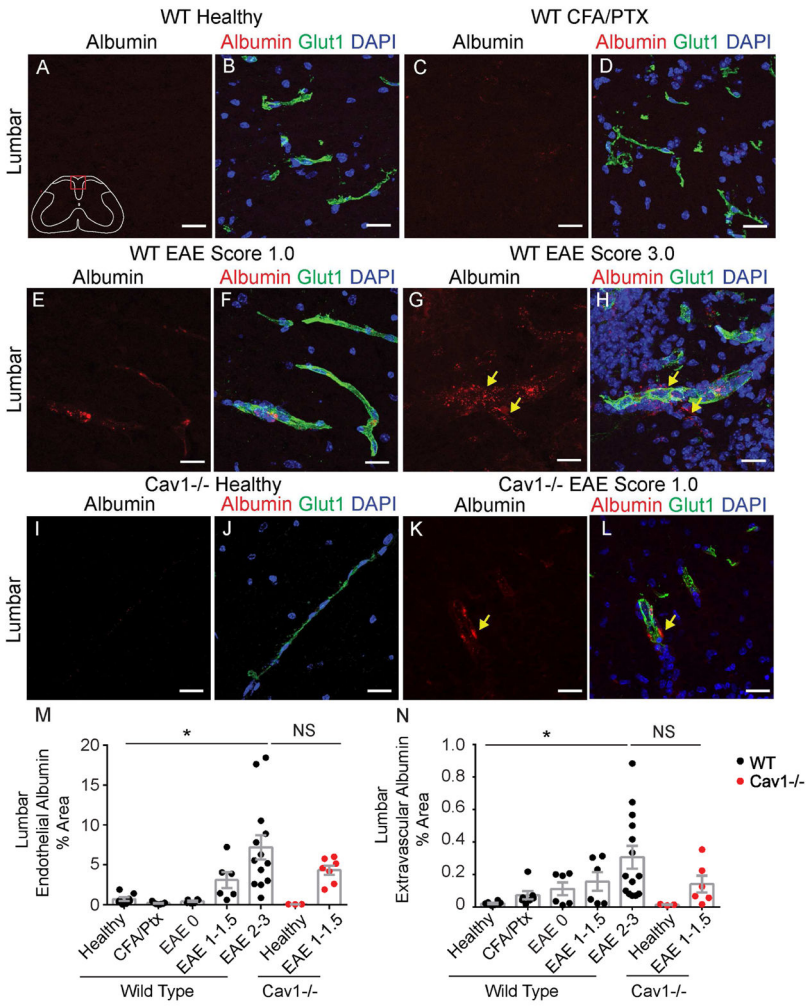

Figure 4. BBB permeability to albumin is increased at peak EAE

A–L) BBB leakage of intravenously injected albumin-AlexaFluor 594 (red) in lumbar spinal cord sections from healthy (A–B), CFA/pertussis toxin control (C–D), EAE scores 1 (E–F) and 3 (G–H) wild-type mice and healthy (I–J) and EAE score 1 (K–L) *Cav1*$^{-/-}$ mice. The vascular marker Glut-1 (green) labels endothelial cells and DAPI (blue) shows nuclei. Yellow arrows indicate perivascular albumin. M,N) Bar graphs of the fraction of endothelium-associated (M) or parenchyma-associated (N) albumin that traversed the BSCB. Each dot represents the mean of multiple fields from a single animal (n = 5–6 healthy, n = 7 CFA/pertussis toxin control, n = 6 EAE score 0, n = 6 EAE score 1–1.5, n = 13–16 EAE scores 2–3, n = 3 healthy *Cav1*$^{-/-}$, n = 7 EAE score 1–1.5 *Cav1*$^{-/-}$). Bar graphs show mean ± SEM, *p<0.05, one-way ANOVA. Scale bars are 20 μm. See also Figure S4.

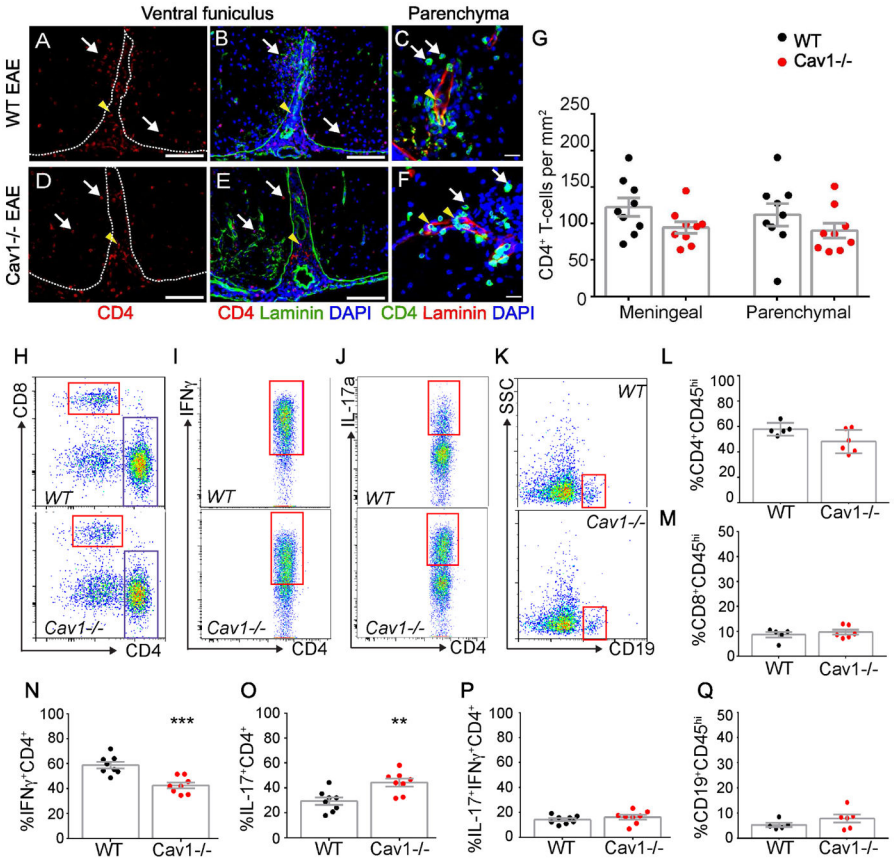

Figure 5. *Cav1* deficient mice have reduced IFN-γ-producing CD4$^+$ T cells in the CNS

A–F) Immunofluorescence for CD4, laminin and DAPI in the ventral (A,B,D,E) and lateral funiculus (C,F) of wild-type and *Cav1*$^{-/-}$ EAE thoracic spinal cords 15 dpi. White arrows point to T cells that have crossed the basal lamina (white dotted line in A,D), whereas yellow arrowheads point to T cells that are located in meningeal or vascular spaces. G) Bar graphs of CD4$^+$ T cell numbers in parenchymal or meningeal compartments of thoracic spinal cords in wild-type and *Cav1*$^{-/-}$ EAE mice 15 dpi. There is no significant difference between genotypes (n = 9 wild-type; n = 9 *Cav1*$^{-/-}$; unpaired two-way Student's t-test). Scale bars in (A,B,D,E) are 200 μm and (C,F) are 10 μm. H–K) FACS plots for mononuclear cells isolated from spinal cords of wild-type (n = 5) or *Cav1*$^{-/-}$ (n = 6) mice 15 dpi. (L–P) Scatter plots of leukocytes gated on viable dye exclusion and high CD45 expression. There were no differences in percentages of infiltrating CD4$^+$ CD45^{hi} (L) or CD8$^+$ CD45^{hi} (M) between the two genotypes. N–O) Significantly fewer IFN-γ-producing CD4$^+$ Th1 cells and significantly more IL-17-producing CD4$^+$ Th17 cells were observed in spinal cords of *Cav1*$^{-/-}$ compared to wild-type mice (n = 8 wild-type, n = 8 *Cav1*$^{-/-}$ mice, *p<0.05, **p<0.01; Student's t-test). P) There is no significant difference in the proportion of IL-17$^+$ IFN-γ$^+$ CD4$^+$ T cells. Q) There was no difference in the fraction of infiltrating CD19$^+$ B cells.

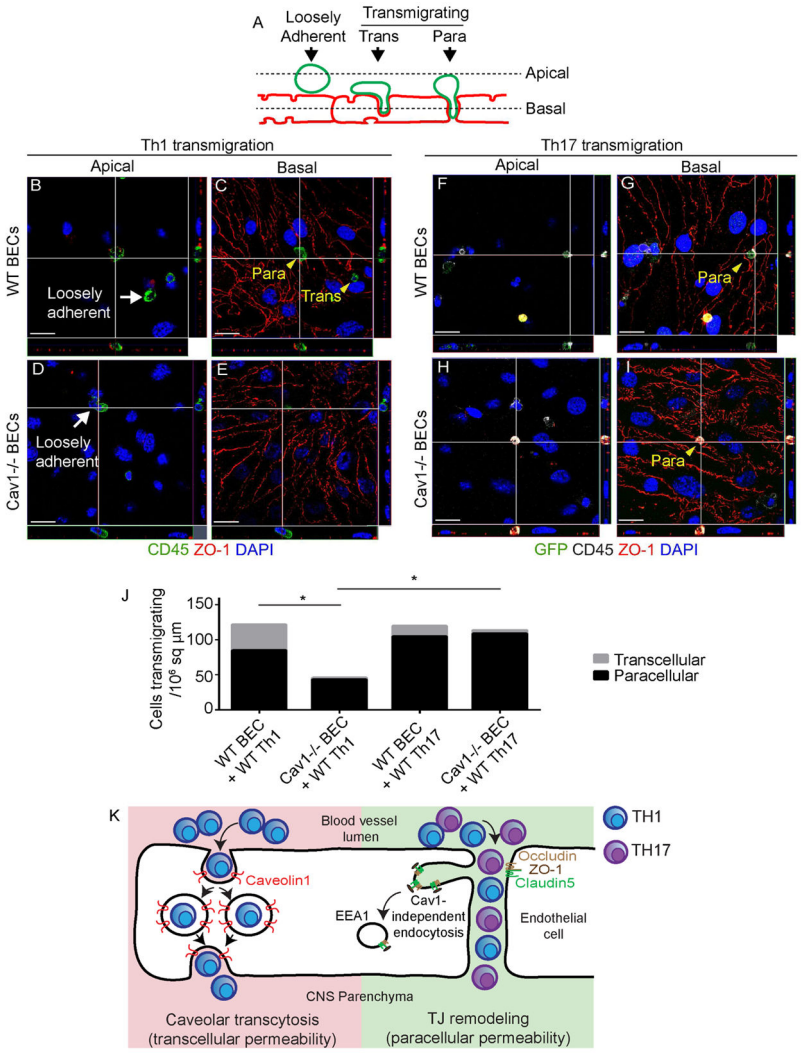

Figure 6. Endothelial Caveolin1 promotes Th1 but not Th17 lymphocyte transcellular transmigration

A) Schematic of T cell transmigration states in the *in vitro* assay. Wild-type Th1 or *Rorc(γt)*$^{GFP/+}$ GFP^{+} Th17 cells were applied to monolayers of wild-type or *Cav1*$^{-/-}$ primary brain ECs (BECs). Based on their positions relative to endothelial ZO-1 in confocal image stacks, T cells were scored as either loosely adherent (non-transmigrating), or transmigrating via transcellular or paracellular routes. B–E) Apical and basal confocal images and orthogonal views of Th1 *in vitro* transmigration assay immunostained for ZO-1 (red), CD45 (green) and DAPI (blue). Loosely adherent Th1 cells are indicated with white arrows and transmigrating Th1 cells with yellow arrowheads on wild-type (B–C) or *Cav1*$^{-/-}$ (D–E) BECs. F–I) Apical and basal confocal images and orthogonal views of *Rorc(γt)*$^{GFP/+}$ Th17 (eGFP^{+}) *in vitro* transmigration assay immunostained for ZO-1 (red), GFP (green), CD45 (white) and DAPI (blue). Scale bar = 10 µm. J) Stacked bar graph indicating numbers of transcellular and paracellular transmigrating Th1 or Th17 cells across wild-type or *Cav1*$^{-/-}$ BECs. Significantly fewer Th1 cells transmigrate across *Cav1*$^{-/-}$ BECs via either transcellular (p<0.05) or paracellular routes (p<0.05) as compared with wild-type BECs.

Significantly fewer Th1 cells transmigrate across *Cav1*$^{-/-}$ BECs as compared with Th17 cells crossing *Cav1*$^{-/-}$ BECs ($p<0.05$). K) Model for lymphocyte trafficking across the BBB in EAE. Th1 cells preferentially deploy caveolae to cross the BSCB (transcellular permeability). In contrast, Th17 cells efficiently cross the BSCB through disrupted TJs (paracellular permeability) as well as caveolae. TJ remodeling involves formation of membrane invaginations (protrusions) that fuse with EEA1^{+} endosomes independently of caveolae. See also Figure S5.